Supporting Information

Rossi et al. 10.1073/pnas.1415467112

SI Text

Depletant Solutions

Attractive forces between superballs were induced by addition of depletion agents with different gyration radii. The depletant dispersions consisted of polymers, microgels, and colloidal particles and each dispersion was prepared and stored as indicated below.

Poly(ethylene oxide). We used poly(ethylene oxide) (PEO) polymer with two different molar masses, namely 6×10^5 g/mol (PEO 600 k) and 7×10^6 g/mol (PEO 7 M), corresponding to a radius of gyration R_g of, respectively, 57 nm and 210 nm (1). The polymer stock solutions of 2 g/L were prepared by dissolving PEO in 10 mM aqueous sodium chloride (NaCl) and they were freshly prepared before microscopy experiments.

Xanthan. Xanthan is a wormlike double-helical polysaccharide with a diameter of ca. 2.2 nm and a persistence length of 120 nm. The stock solution with a final xanthan concentration of 1 g/L was prepared by dissolving xanthan powder (Sigma Aldrich) in water containing 10 mM NaCl and 2 mM sodium azide (NaN_3), the latter to prevent bacterial growth. The mechanically stirred solution was heated to 85 °C using an oil bath and then slowly cooled for about 15 h (2). The xanthan batch used here has a weight-average molar mass M of 3×10^6 g/mol, contour length L_c of about 1.5 μm, and radius of gyration R_g of 329 nm.

Poly(*N*-isopropylacrylamide). Poly(*N*-isopropylacrylamide) (pNIPAM) microgel particles with a radius of 65 nm were prepared following ref. 3. The particles were stored in Millipore water. The total measured mass concentration of the particles in the stock dispersion was 1.22% wt.

Colloidal Akaganèite. Akaganèite (β-FeOOH) rods were prepared following ref. 4. The particles were stored in ethanol at a concentration of about 13% wt. The average length of the rod-like particles was estimated to be 140 nm with a polydispersity of about 30%.

Sample Preparation for Optical Microscopy

Samples with superballs and depletion agents were prepared following the same procedure independently on what depletant was used. First, a small amount of silica superballs (~1 mL), usually stored in ethanol, were sedimented using a microcentrifuge (Beckman Coulter Microfuge 16, typical working speed $1{,}300 \times g$ for about 20 min) and dispersed in water at pH 9; this pH was reached by adding 20–30 μL tetramethylammonium hydroxide 1% wt to 1 mL water. If a dispersion appeared stable under the optical microscope, particles were sedimented and dispersed in 1 mL aqueous solution of 10 mM NaCl, pH 9, containing different depletant dispersions. In samples containing PEO depletant, to prevent PEO adsorption on the surface on the particles, Pluronics F 127 was added to the sample to reach a final Pluronics F 127 concentration of 500 μg/mL. Superballs were dispersed very well and occasionally briefly sonicated. The dispersions were placed into flat VitroCom optical capillaries (0.1 mm × 2 mm × 5 cm) and sealed with UV-sensitive epoxy glue onto clean microscope slides. The samples were allowed to equilibrate for about 20 min before imaging.

Crystal–Crystal Transition

Using pNIPAM depletants alone to induce a crystal–crystal transition poses challenges due to the narrow parameter range that supports suitable interparticle interactions. As the particles shrink at high temperatures, the overall interaction energies decrease considerably, often melting the resulting crystals. Moreover, increasing the number density of the depletant to compensate for the energy loss results in too strong interactions between particles when the depletant is in the expanded state. As a result, it is difficult to achieve the proper conditions for assembly at both the shrunken and expanded states for pNIPAM alone. Thus, crystal–crystal transition experiments were performed using a mixture of pNIPAM and PEO depletants. We used PEO with a molecular weight of 8×10^6 g/mol (PEO 8 M), corresponding to a radius of gyration of ~228 nm (1). pNIPAM microgel particles used in these crystal transition experiments were prepared with no added cross-linker, following ref. 5, and the stock dispersion consisted of the whole reaction dispersion brought to a final NaCl concentration of 10 mM by adding 280 mM NaCl.

Because we were unable to characterize pNIPAM particles using dynamic light scattering, we instead characterized their effect on the assembly of silica superballs. To do that we added 6 μL pNIPAM stock dispersion to 7 μL of a diluted superball suspension, resulting in a total dispersion volume of 13 μL, which was kept at pH 9 and 10 mM NaCl. We find superballs robustly form square lattices at 25.5 °C. When heated to 28.5 °C, we find that depletion interactions weaken considerably, resulting in the complete melting of crystallites. When cooled down once again, the square lattices begin to assemble back (Movie S1).

To test the behavior of superballs dispersed in PEO 8 M we prepared an aqueous dispersion of superballs in 0.31 g/L PEO 8 M, keeping the NaCl concentration at 10 mM and the pH at 9. To prevent adsorption of the PEO onto the surface of the superballs, Pluronics F 127 was added to the sample to reach a final concentration of 500 μg/mL. We find the superballs assemble into Λ_1 lattices (Movie S2).

To perform crystal transition experiments we used a mixture of PEO 8 M and pNIPAM with the same final concentration used for the single depletant experiments reported above. A total of 13 μL of superball dispersion with a final PEO concentration of 0.31 g/L was prepared by mixing 6 μL of the pNIPAM stock dispersion to 7 μL of a superball–PEO 8 M mixture (Movie S3).

Shape Parameters of Silica Superballs

The silica superballs reported in this work (except silica spheres) were obtained by depositing an amorphous silica layer with varying thicknesses starting from the same hematite cores. As the shape parameter m decreased with increasing silica thickness we obtained superballs with $m = 3.9$, $m = 3.5$, and $m = 3.0$, starting from hematite cores having $m \approx 4.0$. Growing an even thicker silica layer would result in superballs with $m < 3.0$. Using these hematite seeds, it is not possible to prepare superballs with $m < 2$.

The contour of a superball is mathematically represented by the formula

$$(x)^m + (y)^m + (z)^m = 1, \qquad \textbf{[S1]}$$

where x, y, and z are Cartesian coordinates and m is the shape parameter, which indicates the extent of deformation. Fig. 1*E* of the main text shows computer-generated models of colloidal superballs with different shape parameters. It is possible to recognize two special cases, which are represented by the sphere for $m = 2$ and the perfect cube for $m = \infty$. All of the intermediate

shape parameters ($m > 2$) correspond to particles having a shape that interpolates between the sphere and the cube. Shape parameters between 2 and 1 correspond to a different family of square-symmetric superballs, whereas shape parameters smaller than 1 correspond to convex solids (6).

To determine the parameters that uniquely characterize the shape of our synthetic particles, we took as a starting point transmission electron microscopy (TEM) images, such as the ones shown in Fig. 1 *B* and *C* of the main text. We then used a standard algorithm to find the edges of the particle and subsequently fitted the edges with the equation

$$\left(\frac{x}{a}\right)^m + \left(\frac{y}{b}\right)^m = 1, \qquad \textbf{[S2]}$$

where a and b are the semiaxes of the particles. Eq. **S2** differs from Eq. **S1** because the analysis is done on TEM images, which are essentially 2D projections of the superballs, and also because Eq. **S2** should account for deviations in the particle aspect ratio (a/b) that, by definition, is 1 for a superball. A typical fit is shown in Fig. 1*B* in the main text and a plot of the results obtained by fitting an ensemble of images (about 100 fits) for different m values is shown in Fig. S1. The average value of m obtained for each superball sample can therefore be used to characterize the roundness of the shape and consequently how much the shape deviates from the cubic shape. The dense cloud of data for the superballs with highest m (sample S3.9, purple points in Fig. S1) indicates that particles are highly monodisperse in shape. The data spread out more for decreasing shape parameter, which is apparently related to the (still poorly understood) mechanism of silica growth on a superball surface. The plot in Fig. S1*B* exhibits for sample S3.0 a curious relation between particle size and shape. The graph shows that for small particle size the sample is monodisperse in shape until a critical particle length is reached (L_c, in this case corresponding to 1.26 μm) at which the shape polydispersity increases. Upon further silica growth beyond the critical length, the shape becomes again monodisperse. The nature of this growth behavior remains to be clarified; the important point here is that despite the polydispersity of samples S3.0 and S3.5, the average position of the data points in Fig. S1 clearly demonstrates that the various superball samples have significantly different average shape parameters.

Bond-Angle Distributions

After particles are allowed to relax, time-lapsed images are collected and analyzed. The particles are identified using an algorithm based on circular Hough transforms. After identifying the positions, we cluster the particles and separate the clusters based on their apparent orientation. For each particle within a cluster, we compute the angles between adjacent nearest-neighbor bonds. An ensemble of bond angles is collected over time and over each particle within a cluster.

The bond-angle distributions are used to identify which of the lattice type of interest are statistically most similar to the experimental structures. This is accomplished by comparing the resulting distributions to the values of the bond angles expected for the square, Λ_0, and Λ_1 lattices for the particular value of m. Fig. S2*A* shows the distribution of bond angles for experimental data corresponding to a variety of shape parameters. For experiments characterized by broad distributions of bond angles (Fig. S2 *C* and *D*), a clear identification may not be possible.

Predicted Phase Diagram

The bound state energy of a superball inside of a depletion-stabilized lattice is given by $U = -nK_BT\Delta V_{ex}$, where ΔV_{ex} is the change in volume excluded when a particle is removed from the interior of an otherwise filled lattice and n is the number density of depletants. This volume change is computed by first constructing a finely pixelated binary image of an arrangement of filled outlines of superballs of length $L + R_g$ placed at the lattice sites corresponding to square, Λ_0, and Λ_1 lattices for fixed L and shape parameter m. Similar images are produced corresponding to the same arrangement with one particle removed from the interior of the lattice. ΔV_{ex} is computed by subtracting the total number of nonzero pixels for the full lattice by the lattice with one particle missing and then subsequently subtracting the number of nonzero pixels for an isolated superball of length $L + R_g$. By computing and comparing ΔV_{ex} for the Λ_0, Λ_1, and square lattices, we estimate which lattice is energetically favorable for a particular value of m (Fig. S3 *A* and *C*).

To quantify how energetically favorable a particular lattice is for a particular m and q, we also compute the difference in energy between the two lattices that have the lowest values. This difference characterizes the energetic benefit of choosing one particular lattice. When the difference is zero, the most favorable lattices becomes degenerate.

To compare the energetics in different regions of the phase diagram, however, a consistent definition of the number density of depletants n must to be used. Fig. S3*E* shows the diagram computed using a constant depletant density between experiments. In our experiments, the depletant concentration is typically on the order of C^*, where C^* is maximum density in which the depletants can maintain their radius of gyration. We thus use $n \propto 1/V_{dep}$, where V_{dep} is the volume of the depletant. Fig. S3 *B* and *D* shows the resulting diagram, which corresponds to normalizing the difference in ΔV_{ex} by the volume of the depletant. We note that this simple model neglects to account for the rotational and vibrational entropy of the superballs.

Fig. S3 *C* and *D* corresponds to diagrams computed for 2D arrangements of 3D superballs. The complementary diagrams for purely 2D superdisks are shown in Fig. S3 *A* and *B*. The qualitative similarity reflects the quasi-2D nature of the system.

Simulation Details

We consider colloidal superballs with a surface satisfying the equality

$$|x|^m + |y|^m + |z|^m = \left(\frac{\sigma_c}{2}\right)^m, \qquad \textbf{[S3]}$$

where σ_c is the superball diameter at its narrowest point and m controls the particle shape as described in the main text. The rounded cubes are treated as hard particles with no attraction or repulsion and are confined to move in a 2D plane to mimic moving on a substrate. The depletants may move in all three dimensions and are modeled as penetrable spheres of diameter $\sigma_d = 2R_g$, with R_g the radius of gyration of the polymer depletant, that may overlap with one another but not with the superballs. Overlap is detected using the algorithm of Donev (7) as implemented in ref. 8.

For all simulations described here we study a fixed number, N, of superballs and the depletant particles are treated grand canonically with a constant chemical potential, μ_d, corresponding to a fixed reservoir volume fraction, η_d^r. Instead of the depletant diameter we quote the size ratio, $q = \sigma_d/\sigma_c$, which we study in the range $0.04 \le q \le 0.35$. The volume fraction, η_d^r is related to reservoir number density by

$$\eta_d^r = \frac{n_d^r \pi \sigma_c^3 q^3}{6} \qquad \textbf{[S4]}$$

and from here on we quote reservoir number density.

The difficulty in simulating highly size-asymmetric binary mixtures is that rearrangements of the large particles (the ones we are most interested in) are limited by the length scales of the smaller particles. To remediate this problem we use the geometric cluster algorithm (GCA) of Dress and Krauth (9), later extended by Liu

and Luijten (10). In this method a large particle is added to the cluster and moved using a self-inverse operation, such as reflection in a point pivot. After this move, any particles overlapping are also added to a cluster. At each iteration a particle is taken off the bottom of the stack and moved, repeating until all particles have been moved or no overlaps remain. Clusters may move an arbitrary number of large particles or can be limited to one large particle. Rearrangement of large clusters is vital in the early stages of self-assembly, whereas single-particle moves are more efficient for relaxing particles within an assembled structure.

Special consideration is required for moving anisotropic particles such as the superballs considered here. As described in ref. 11, we include a GCA move that reflects a large particle in a plane instead of a point pivot as shown in Fig. S4. If the plane lies close to one of the superball's axes, then the rotation can be arbitrarily small. This allows the large particles to fully explore their orientational degrees of freedom. Our full move set is as follows: Each Monte Carlo sweep we attempt on average one large cluster move and N single-particle moves. For the single-particle moves the reflection pivots and planes are chosen close to the target particle to increase the acceptance rate.

Even using the GCA simulations is challenging for a number of reasons: The interactions are strong and short ranged, which makes assembly difficult with very long physical timescales. Computationally the overlap checks with superballs are expensive and often require slowly converging numerical solvers. The large number of depletants means that many overlap checks need to be made. In particular, to observe transitions between states in a reasonable timescale, care has to be taken to choose parameters that do not create interactions that are too strong, leading to kinetic trapping, while strong enough to allow assembly.

Self-Assembly Simulations

To study the formation of self-assembled structures we place $N = 169$ superballs evenly distributed in a periodic box of dimensions $L_x = L_y = 30\sigma_c$ and $L_z = 1.05\sigma_c$. The box is filled with depletants grand canonically before the large particles are allowed to move. The simulation is then run until the assembled structures are stable to rearrangement. We studied a range of particle shapes, m, and depletant size ratios, q, and for each combination scanned a range of depletant number densities, n_d^r to find the point of best assembly. We found that the window between the interactions being too weak for assembly and too strong for good assembly (kinetic trapping) was quite narrow due to the short-ranged nature of the depletion interaction.

The final configurations are shown in Fig. S5, indicating the different structures that assemble for different combinations of shape and depletant size. The simulations suffer from kinetic trapping, in particular when the depletant is small, in a manner quite similar to that seen in experiments. The stable structures from these simulations generally agree with the experimental results. The results are summarized and compared with the experiment in Fig. S6.

Bulk Phase Simulations

To better understand which phase, square or Λ_1, is truly thermodynamically stable we also performed simulations in the bulk to remove surface effects. Simulations were performed in the $NPT\mu_d$ ensemble at a constant pressure, P, and fluctuating box size. The box shape was also allowed to fluctuate (sometimes referred to as a "floppy box") to accommodate crystal structures that do not tile in a square box. The pressure, P, is set by the depletant pressure in the reservoir, that of an ideal gas $\beta P = n_d^r$ where n_d^r is the reservoir depletant number density and β is the inverse of temperature multiplied by Boltzmann's constant, $\beta = (k_B T)^{-1}$, which is far higher than the pressure from the superballs. In this ensemble it is possible for the box to increase to an arbitrarily large size if the depletion interaction is not strong enough. If the superballs are started sufficiently close together, this does not represent a practical problem.

We placed $N = 6 \times 6 = 36$ superballs in a periodic box. The values for n_d^r and hence also the pressure were chosen to match the values at which we see good assembly in the previous section. To determine which phase is stable for any given set of parameters we started simulations from square, Λ_0, and Λ_1 phases. Example configurations are shown in Fig. S7.

Bidepletant

In this section we demonstrate the possibility of switchable phases by considering a system made up of superballs and two species of depletant. The big depletants are spheres with size ratio $q_1 = 0.35$ and the small depletants are spheres with size ratio $q_2 = 0.04$. Both depletants can overlap with each other but not with the superballs. The changes in size always occur at constant reservoir number density so that the average number of small depletants remains constant throughout the simulation. This is an average because the depletants are treated grand canonically and their numbers fluctuate.

Self-Assembly. In this ensemble the number of superballs is fixed at $N = 169$ and the box size is constant at $L_x = L_y = 30\sigma_c$ and $L_z = 1.02\sigma_c$. Both depletants are treated grand canonically with constant chemical potentials, μ_1 and μ_2. The simulations start with all of the superballs evenly distributed and the box filled with depletant. Although there is potentially a large parameter space, we have found that starting with $q_1 = 0.35$ and $q_2 = 0.04$ and at reservoir number density $n_1 = 24.9\sigma_c^{-3}$ and $n_2 = 596.8\sigma_c^{-3}$ provides the best results.

As shown in Fig. S8 under the starting conditions the superballs assemble into a square structure. Even though the amount of small depletant would not be strong enough to drive assembly on its own, with the help of the larger depletant to hold the particles together it is enough to direct the superballs into a square phase. At this point the size of the small depletant is changed from $q_2 = 0.04$ to $q_2 = 0.032$, holding the number density fixed, resulting in a canted lattice. When the small depletants are swollen back to $q_2 = 0.04$, the square phase is restored, demonstrating a mechanism that induces reversibly switchable phases.

We note that to see transitions in a computationally accessible timescale, the parameters must be chosen such that the interactions are not too strong. Due to the weaker and competing interactions, the bond angles that we see in the canted phase are slightly different from those in the close-packed Λ_1 phase.

Bulk Phase. This is a constant $NPT\mu_2$ ensemble. N is the number of superballs. The pressure is set by the depletant pressure in the reservoir, which is far higher than pressure from the superballs. Because the reservoir is an ideal gas, the reservoir pressure is the sum of the depletant number densities, $\beta P = n_1 + n_2$. The big depletants are too big to penetrate the crystal structure so although it contributes to the pressure, it is not explicitly simulated in this ensemble. As in the previous bulk section, as well as in volume-changing moves (L_x and L_y only), the box may also make shape-changing moves. This allows the Λ_1 phase to properly fit around the periodic boundaries.

The contribution to the pressure from the big depletant is fixed at $\sigma_c^3 \beta P_1 = 30$. The box is filled with small depletant with $q_2 = 0.04$ at $n_2^r = 596.8\sigma_c^{-3}$, so the total pressure is $\beta P = \beta(P_1 + P_2) = 626.8$. The number densities remain fixed so this pressure is the same in all results shown here.

Fig. S9 shows the switchable nature of the crystals. The superballs are started in a square configuration and then the box is filled with depletant at $q_2 = 0.04, n_2^r = 596.8\sigma_c^{-3}$, where the square phase is stable. The small depletant is then changed in size to $q_2 = 0.032$ and the system reliably changes into the canted phase. From this configuration the small depletant size is changed back to $q_2 = 0.04$, and the crystal changes back to the square (Movie S4).

1. Devanand K, Selser JC (1991) Asymptotic behavior and long-range interactions in aqueous solutions of poly(ethylene oxide). *Macromolecules* 24:5943–5947.
2. Koenderink GH, Sacanna S, Aarts DGAL, Philipse AP (2004) Rotational and translational diffusion of fluorocarbon tracer spheres in semidilute xanthan solutions. *Phys Rev E Stat Nonlin Soft Matter Phys* 69(2 Pt 1):021804.
3. Pelton RH, Chibante P (1986) Preparation of aqueous latices with N-isopropylacrylamide. *Colloids Surf* 20:247–256.
4. Sacanna S (2007) Novel routes to model colloids: Ellipsoids, latices and stable meso-emulsions. PhD thesis (Utrecht University, Utrecht, The Netherlands).
5. McPhee W, Tam KC, Pelton R (1993) Poly(N-isopropylacrylamide) latices prepared with sodium dodecyl sulfate. *J Colloid Interface Sci* 156(1):24–30.
6. Jiao Y, Stillinger FH, Torquato S (2009) Optimal packings of superballs. *Phys Rev E Stat Nonlin Soft Matter Phys* 79(4 Pt 1):041309.
7. Donev A (2006) Jammed packings of hard particles. PhD thesis (Princeton University, Princeton).
8. Ni R, Gantapara AP, de Graaf J, van Roij R, Dijkstra M (2012) Phase diagram of colloidal hard superballs: From cubes via spheres to octahedra. *Soft Matter* 8:8826–8834.
9. Dress C, Krauth W (1995) Cluster algorithm for hard spheres and related systems. *J Phys Math Gen* 28:L597–L601.
10. Liu J, Luijten E (2004) Rejection-free geometric cluster algorithm for complex fluids. *Phys Rev Lett* 92(3):035504.
11. Ashton DJ, Jack RL, Wilding NB (2013) Self-assembly of colloidal polymers via depletion-mediated lock and key binding. *Soft Matter* 9:9661–9666.

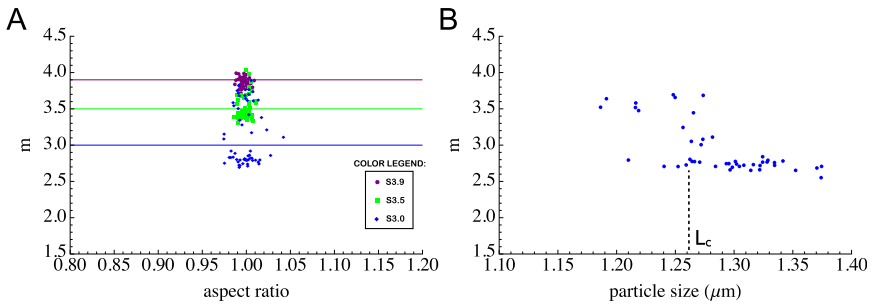

Fig. S1. (*A*) The points of this graph represent the shape parameters *m* of the silica superballs measured by fitting the shape of 80–100 particles. Different colors correspond to different samples as indicated in the legend. The average values are indicated with the horizontal lines interpolating the *y* axis in their corresponding mean values. (*B*) For sample S3.0 the shape parameter (*m*) of the particle is plotted against the particle size (*L*). A sharp transition is visible around a critical value $L_c = 1.26$ μm, which shows a rapid decay in shape polydispersity after the transition.

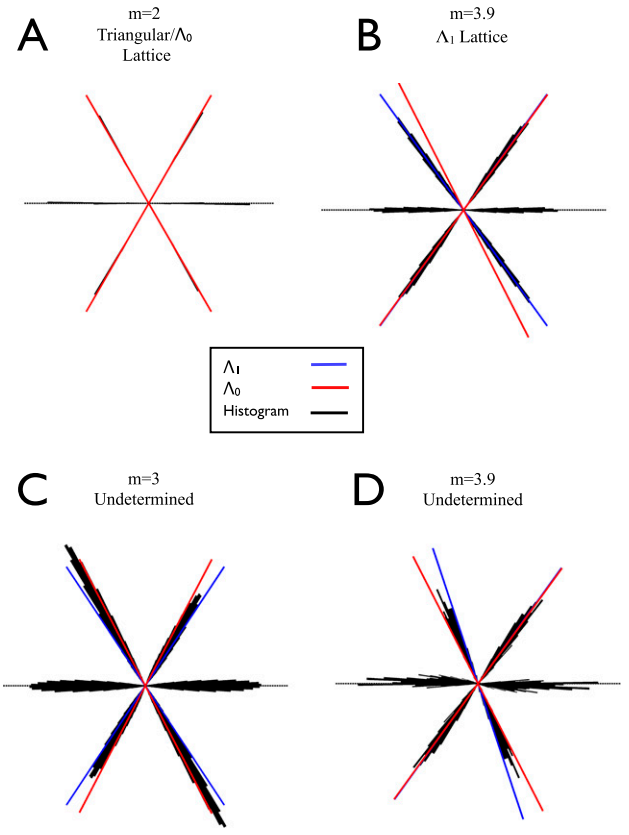

Fig. S2. Angular histograms of experimental data. (*A*) Angular histograms for spherical particles show sharp peaks indicating 60° bond angles between particles, as expected for a triangular lattice, which is consistent with both the Λ_0 and Λ_1 lattices for $m = 2$. (*B*) Example angular histogram from which a Λ_1 lattice is identified. *C* and *D* show examples of distributions in which a clear identification is not possible.

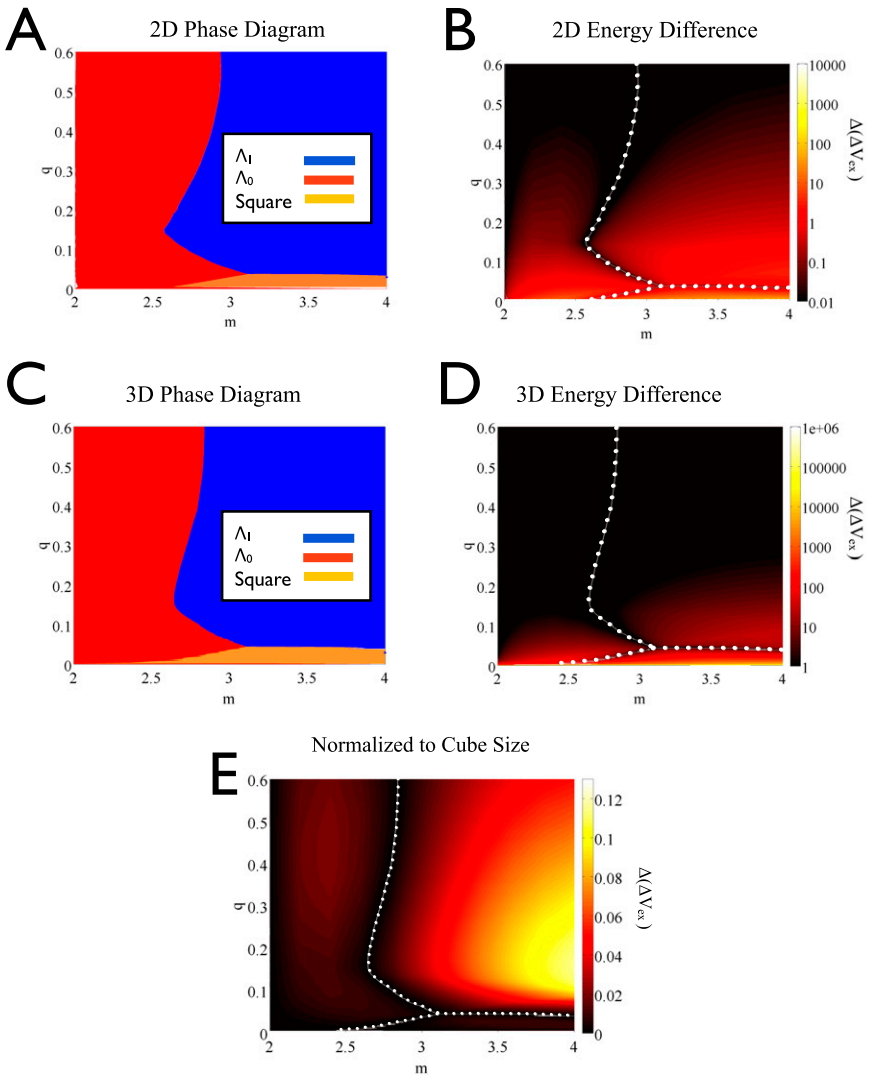

Fig. S3. Phase diagrams and energetic characterization of superball lattices. (*A*) The phase diagram of 2D superdisks is computed by computing ΔV_{ex} of each lattice type for each value of m and q. (*B*) The energetic benefit of choosing a particular lattice type for 2D superdisks is computed for each m and q by finding the difference in the energy of the two most energetically favorable lattices. (*C* and *D*) Phase diagram for 3D superballs arranged in 2D lattices. The structures of the diagrams are qualitatively similar to those of the 2D diagrams. (*E*) The energy difference between the two most favorable lattices computed using a constant number density of depletants.

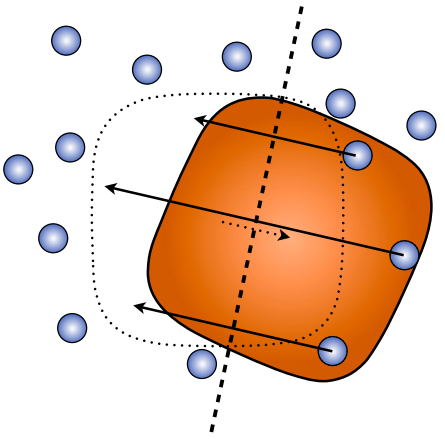

Fig. S4. Starting from the dotted outline the colloid particle is reflected in the plane (thick dashed line). As a result it overlaps with three depletant particles that are reflected in the same plane into the space left by the colloid.

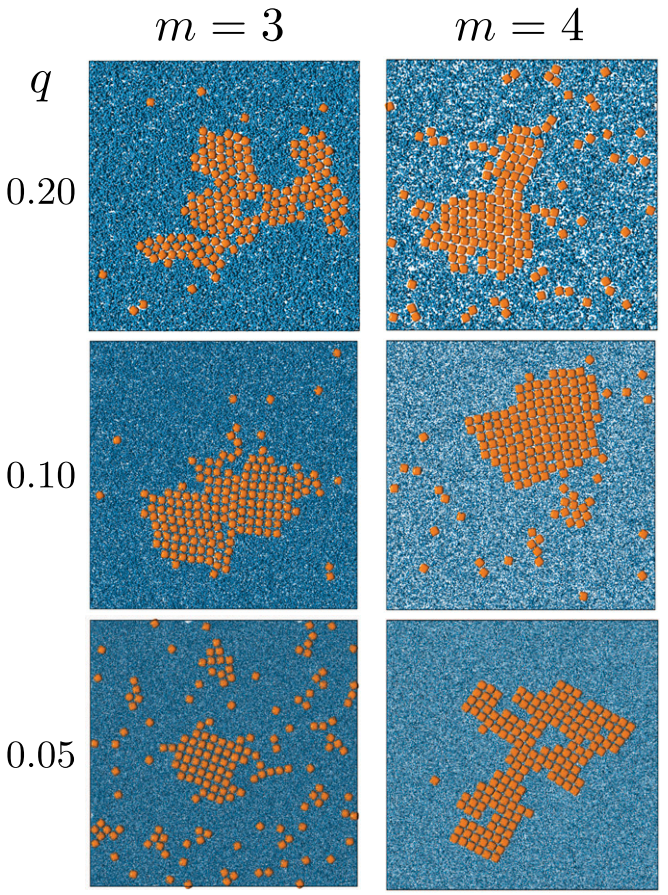

Fig. S5. Final configurations for the self-assembly simulation runs for varying size ratios q and superball shape parameter m as labeled.

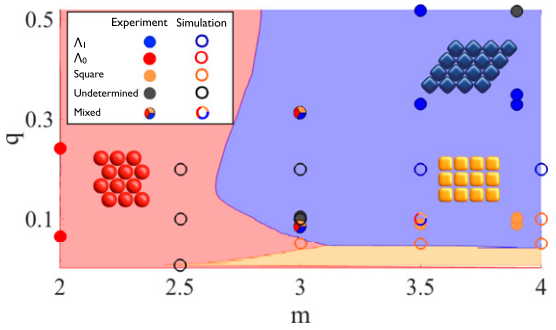

Fig. S6. Comparison of finite crystal self-assembly simulation results with experiment results.

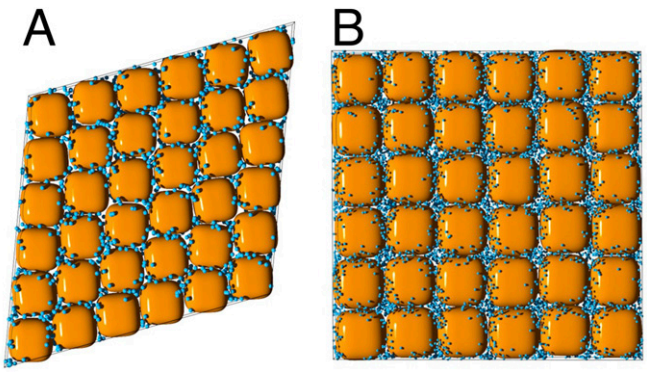

Fig. S7. (*A* and *B*) Floppy box *NPT* simulations showing the stable structures for superballs with shape parameter $m = 3.5$ (*A*) Λ_1 phase for size ratio $q = 0.1$ and (*B*) square phase for $q = 0.05$.

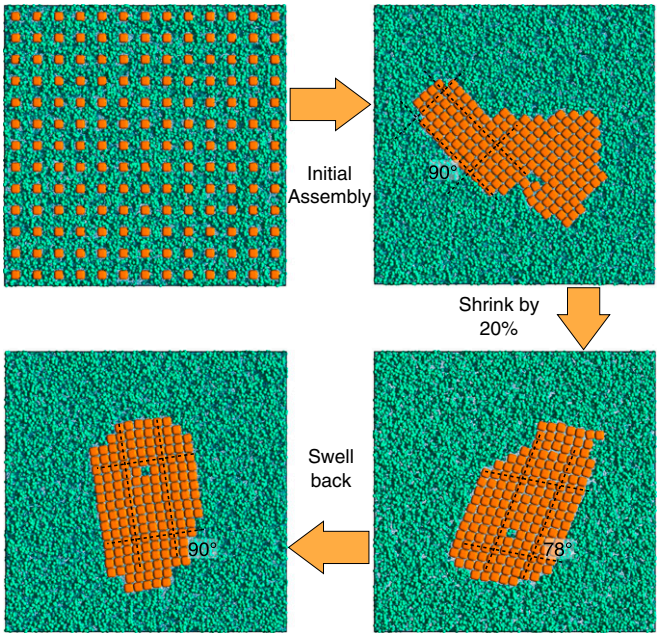

Fig. S8. After initial assembly into a square phase the small depletant is shrunk by 20% from $q_2 = 0.04$ to $q_2 = 0.032$, holding the densities of both depletant species and superballs fixed. The crystal rearranges to a canted phase. The depletant then goes back to $q_2 = 0.04$ and the square phase is recovered.

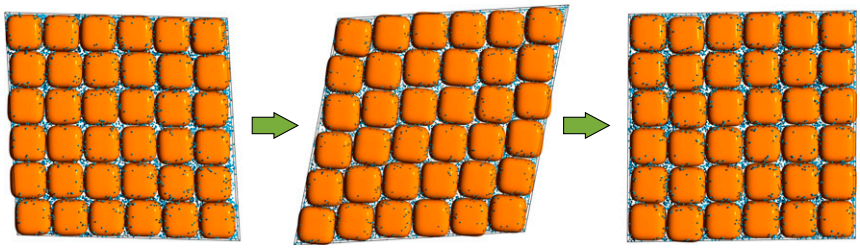

Fig. S9. Constant pressure simulations with a flexible "floppy" box. Starting from a square phase we cycle to a Λ_1 phase and back again by changing the small depletant size from $q_2 = 0.04 \rightarrow 0.032 \rightarrow 0.04$ at constant number density. The big depletants do not penetrate the crystal so are treated implicitly as a pressure term.

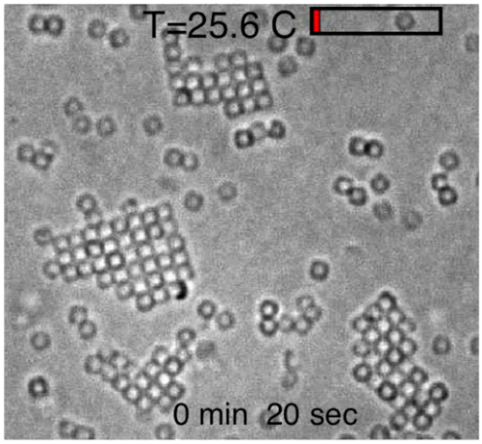

Movie S1. Silica superballs with $m = 3.9$ are dispersed with pNIPAM depletants and equilibrated at room temperature, where they form square crystallites. As the temperature is increased to 28.5 °C, the crystallites melt. Upon decreasing the temperature back to room temperature, the particles begin to reassemble.

Movie S1

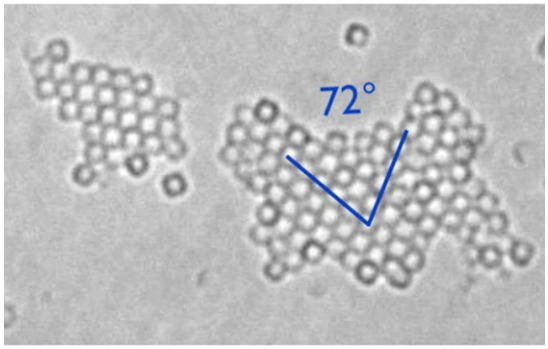

Movie S2. Silica superballs with $m = 3.9$ are dispersed in the presence of PEO depletants with molecular weight 8 M. In these conditions the superballs assemble into Λ_1 crystallites.

Movie S2

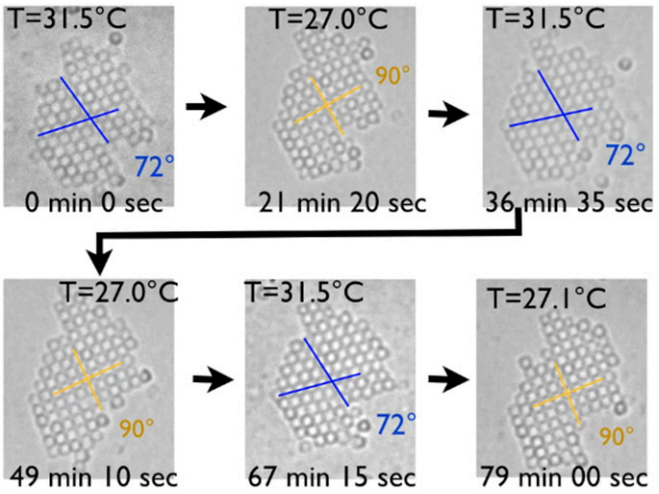

Movie S3. Silica superballs with $m = 3.9$ are dispersed in the presence of a mixture of PEO (molecular weight 8 M) and pNIPAM depletants. At 27 °C, the superballs assemble into square crystallites, as observed when the particles are dispersed with pNIPAM alone. As the temperature is increased we observe that the lattice shifts to a Λ_1 configuration as observed when the superballs are dispersed with PEO alone. This happens because at higher temperatures the interactions induced by the pNIPAM weaken whereas those induced by the PEO are fixed. By cycling the temperature, we are able to observe a reversible solid-to-solid phase transition over several iterations.

Movie S3

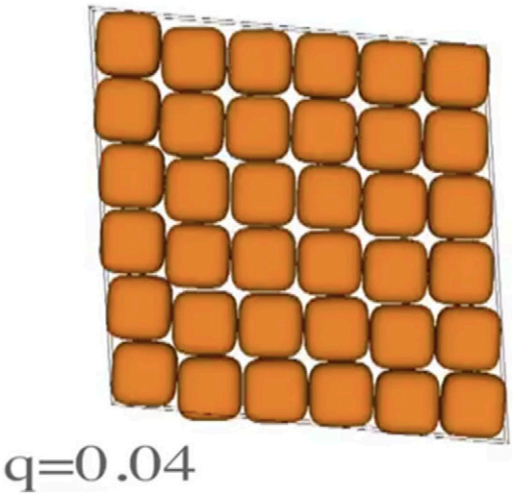

Movie S4. Periodic bulk crystal simulations are performed with superballs with a fluctuating simulation box. Superballs are dispersed with two species of depletants, one with size ratio $q_1 = 0.35$ and one with size ratio $q_2 = 0.04$. For these parameters, The square lattice configuration is stable. By decreasing the size ratio of the smaller species from $q_2 = 0.04$ to $q_2 = 0.032$, we observe a transition into a canted phase, as we observe when the superballs are dispersed only with depletants with a size ratio $q_1 = 0.35$. When the size of the smaller depletant is once again increased ($q_2 = 0.04$), the square phase is restored.

Movie S4